# SAR439859, a Novel Selective Estrogen Receptor Degrader (SERD), Demonstrates Effective and Broad Antitumor Activity in Wild-Type and Mutant ER-Positive Breast Cancer Models

Maysoun Shomali[1], Jane Cheng[1], Fangxian Sun[1], Malvika Koundinya[1], Zhuyan Guo[1], Andrew T. Hebert[1], Jessica McManus[1], Mikhail N. Levit[1], Dietmar Hoffmann[1], Albane Courjaud[2], Rosalia Arrebola[2], Hui Cao[1], Jack Pollard[1], Joon Sang Lee[1], Laurent Besret[2], Anne Caron[2], Dinesh S. Bangari[3], Pierre-Yves Abecassis[2], Laurent Schio[2], Youssef El-Ahmad[2], Frank Halley[2], Michel Tabart[2], Victor Certal[2], Fabienne Thompson[2], Gary McCort[2], Bruno Filoche-Rommé[2], Hong Cheng[1], Carlos Garcia-Echeverria[2], Laurent Debussche[2], and Monsif Bouaboula[1]

## ABSTRACT

Primary treatment for estrogen receptor-positive (ER+) breast cancer is endocrine therapy. However, substantial evidence indicates a continued role for ER signaling in tumor progression. Selective estrogen receptor degraders (SERD), such as fulvestrant, induce effective ER signaling inhibition, although clinical studies with fulvestrant report insufficient blockade of ER signaling, possibly due to suboptimal pharmaceutical properties. Furthermore, activating mutations in the ER have emerged as a resistance mechanism to current endocrine therapies. New oral SERDs with improved drug properties are under clinical investigation, but the biological profile that could translate to improved therapeutic benefit remains unclear. Here, we describe the discovery of SAR439859, a novel, orally bioavailable SERD with potent antagonist and degradation activities against both wild-type and mutant Y537S ER. Driven by its fluoropropyl pyrrolidinyl side chain, SAR439859 has demonstrated broader and superior ER antagonist and degrader activities across a large panel of ER+ cells, compared with other SERDs characterized by a cinnamic acid side chain, including improved inhibition of ER signaling and tumor cell growth. Similarly, *in vivo* treatment with SAR439859 demonstrated significant tumor regression in ER+ breast cancer models, including MCF7-*ESR1* wild-type and mutant-Y537S mouse tumors, and HCI013, a patient-derived tamoxifen-resistant xenograft tumor. These findings indicate that SAR439859 may provide therapeutic benefit to patients with ER+ breast cancer, including those who have resistance to endocrine therapy with both wild-type and mutant ER.

## Introduction

Antihormonal therapies that directly antagonize the function of the estrogen receptor alpha (ERα; such as tamoxifen) or therapies that block the production of its ligand, estrogen (such as aromatase inhibitors), are the mainstay therapy for ER-positive (ER+) breast cancer (1–4). Although these treatments markedly reduce the risk of recurrence from early-stage disease and improve outcomes in patients with advanced disease, relapse frequently occurs after prolonged treatment (1, 4–6). Recently, recurrent mutations have been identified in the ligand-binding domain of ERα in approximately 25% to 40% of patients who have relapsed after receiving one or more prior hormonal therapies (7–10). These mutations confer estrogen-independent, constitutive activity of the ERα, induction of tumor growth, reduced potency to anti-ERα therapies, and complete resistance to aromatase inhibitors (7–10).

Some ligands that target the ERα can increase levels of the ERα protein steady state due to biological feedback mechanisms such as increases in the transcriptional compensation or thermodynamic stability upon ligand binding (11). For example, tamoxifen induces stabilization of the ERα protein, which adopts a conformation that may lead to agonist signaling (12–16). It has also been suggested that some mutations in the ERα, such as those affecting the Y537S or D538G amino acids, may be involved in stabilization of the ERα (10, 16–19). Moreover, an increase in ERα stability could also result in ERα signaling leakage when continuous treatment coverage is not achieved. Altogether, there is rationale, in addition to ERα antagonism, that degradation of the ERα protein could have an impact on the ERα biology and efficacy of therapies targeting ERα.

Selective estrogen receptor degraders (SERD), such as fulvestrant, bind to the ERα to induce a conformational change that not only antagonizes ERα function, but also causes its proteasome-mediated degradation to more effectively inhibit ERα signaling. Fulvestrant is an approved SERD indicated for the treatment of ER+ metastatic breast cancer in postmenopausal women with disease progression following anti-estrogen therapy (20). Fulvestrant has demonstrated preclinical and clinical benefits after failure of other hormonal therapies (21–23). However, fulvestrant, a steroid with a neutral and lipophilic side

[1]Sanofi, Research and Development, Cambridge, Massachusetts [2]Sanofi, Research and Development, Vitry-sur-Seine, France. [3]Sanofi, Research and Development, Waltham, Massachusetts.

**Note:** Supplementary data for this article are available at Molecular Cancer Therapeutics Online (http://mct.aacrjournals.org/).

**Corresponding Author:** Maysoun Shomali, Sanofi (United States), 640 Memorial Drive, Cambridge, MA 02478. Phone: 617-665-4945; E-mail: maysoun.shomali@sanofi.com

Mol Cancer Ther 2021;20:250–62

**doi:** 10.1158/1535-7163.MCT-20-0390

chain, requires unconventional long-acting intramuscular depot formulation, limiting its dose and exposure for maximal receptor engagement (24, 25).

To address the preceding pharmacologic shortcomings posed by fulvestrant, several novel SERDs have entered clinical trials including GDC-0810 (NCT 01823835), AZD9496 (NCT02248090), AZD9833 (NCT03616586), GDC-0927 (NCT02316509), and GDC-9545 (NCT03916744, NCT03332797; refs. 26–28). These novel SERDs, which are chemically distinct from fulvestrant, can be classified into two major groups based on the chemical structure of their side chain that is key in driving ERα degradation (29–31). GDC-0927 is characterized by a fluoroalkylamine side chain, whereas GDC-0810, AZD9496, and LSZ102 each have a cinnamic acid side chain (26, 27, 29, 32–34). It is not well understood whether the different side chains and/or their abilities to induce ERα degradation translate to differences in their biology and antitumor activities. Moreover, these SERDs have presented conflicting data in their relative abilities to induce ERα agonist activity or promote complete ERα degradation (26, 28, 35).

To better define the molecular features to achieve optimal clinical activity of SERDs, it is crucial to understand the relationship between the molecular structure of the drug, level of ERα degradation, and the subsequent impact on antitumor activity. Here, we describe SAR439859, a novel, nonsteroidal, orally bioavailable SERD that bears a fluoropropyl pyrrolidinyl side chain and, unlike SERDs with a cinnamic acid side chain, SAR439859 has demonstrated strong ERα antagonist activity and potently induces its degradation, which results in improved efficacy of both *in vitro* and *in vivo* ER+ breast cancer models.

## Materials and Methods

Key details of the materials and methods used in this study are provided below (see Supplementary Appendix for additional information). Animal studies were conducted in accordance with the Guide for the Care and Use of Laboratory Animals, National Academy Press (2006), conforming to Massachusetts State legal and ethical practices and approved by the Institutional Animal Care and Use Committee (IACUC, Sanofi Genzyme).

### Cell culture and reagents

MCF7, CAMA-1, ZR-75–1, MDAMB134VI, MDAMB361, BT474, BT473, MDAMB415, EFM19, HCC1428, HCC1500, HEK293T, MDAMB231, and SUM44PE cells were purchased from ATCC or Asterand and underwent authentication using short tandem repeat (STR) DNA profiling at Idexx. The HCC1428 LTED cell line was obtained from Carlos Arteaga. All cell lines were routinely screened for mycoplasma contamination using Lonza Mycoalert and Stratagene Mycosensor. Unless otherwise indicated, tissue culture supplements and medium were purchased from Hyclone, Corning, or Invitrogen. Cells were maintained as recommended by ATCC. HCC1428-LTED was maintained in phenol red-free IMEM with 10% dextran-charcoal-treated (CSS) FBS. SUM44PE was maintained as previously described in IMEM with 2% CSS (36). Generation and maintenance of primary tumor xenografts was described previously (37). HCI-013 was established from a pleural effusion in a 53-year-old woman with metastatic ER+/progesterone receptor-positive/human epidermal growth factor receptor 2-negative invasive lobular carcinoma (gifted from Alana Welms). Fulvestrant, 4OH-tamoxifen, raloxifene, bazedoxifene, and 17β-estradiol were purchased from Sigma-Aldrich.

### Compounds

SAR439859 was synthesized as described in WO2017140669, as Example 51 (38). GDC0810 and AZD9496 were synthesized as described in WO2012037410 (Example 111; ref. 39) and WO2014191726 (Example 1; ref. 40), respectively. Both AZD-SAR and GDC-SAR were made as described in WO2018091153 (Example 255 and 256, respectively; ref. 41).

### In-cell Western assay

MCF7 cells were seeded at a density of 15,000 cells per well into flat clear bottom tissue cultured-treated 384-well plates (Corning) in IMEM with 5% CSS FBS. After treatment with ligand at the indicated concentrations, plates were washed, fixed 10% with neutral buffered formalin, permeabilized with PBS containing 0.1% Triton X-100, and blocked with Odyssey Blocking Buffer (LI-COR). The fixed cells were incubated with rabbit anti-ERα antibody (SP-1; MA5-14501; Thermo Fisher Scientific), washed and stained with Alexa Fluor 488 goat anti-rabbit secondary antibody (Invitrogen) and Hoechst DNA stain to determine cell number. ERα levels were quantitated using the acumen eX3 imaging system. Percent residual ERα was defined as normalized ERα treated cells/normalized ERα untreated cells $\times 100$.

### Simple Western assay

Cells and tissues were lysed with an RIPA buffer (Boston BioProducts) or with tissue protein extraction reagent with Halt protease inhibitors and EDTA (Thermo Fisher Scientific), respectively. Proteins from cell or tissue lysates were separated by capillary electrophoresis using the Simple Western assay (ProteinSimple), as described previously (29) and probed with rabbit anti-ERα antibody (Cell Signaling Technologies, 13258) and β-actin (Cell Signaling Technologies, 3700). ERα levels were quantitated using the Compass software (ProteinSimple); percent ERα was calculated by normalizing ERα values to β-actin and then expressed as a percentage of the normalized value of the untreated cells.

### Viability assays

Trypsinized cells were dispensed into 384-well plates in IMEM (supplemented with 5% FBS) and after overnight incubation cells were treated with compounds for the times indicated. Cell viability was assessed using CellTiter-Glo (Promega) according to the manufacturer's protocol and relative luminescence units (RLU) were measured using an Envision Multilabel Reader (Perkin Elmer). The RLUs of the treated samples were normalized to that of the untreated samples and cell viability was expressed as a percentage of the value of the untreated cells.

### Mutant ERα cell line generation

*ESR1* was cloned from a brain cDNA library. ERα mutant plasmids Y537S and D538G were generated using Quik Change II Mutagenesis Kit (Agilent) *ESR1* wild-type and mutant complementary DNAs were subcloned into a lentivirus plasmid containing an amino terminal hemagglutinin (HA) tag lentivirus plasmid (pLenti9 or pLenti6.3). Lentiviral supernatants were generated by transfection of a lentivirus plasmid encoding ERα mutants Y537S and D538G in HEK293T cells using a packaging mix (Cellecta), according to the manufacturer's protocol. After transfection, lentiviral particles were purified from the cell medium and MCF7 target cells were transduced with lentiviral supernatants with 8 μg/mL polybrene (Millipore Sigma). Stable cell lines were selected for 5 μg/mL blasticidin resistance. Cells were characterized for constitutive or doxycycline-inducible ER expression using Simple Western blot, as described previously. HA-tagged mutant

ERα was confirmed by Western blot analysis using the 6E2 mouse monoclonal anti-HA antibody (Cell Signaling Technology, 2367).

### Recombinant ER proteins

Recombinant proteins representing amino acids 289–554 of the ligand-binding domain (LBD) of human ERα with the $His_6$-tag at the N-terminus ($His_6$-ERα-LBD) were synthesized by DNA 2.0 and cloned in pBH4743 vector. They were expressed in *Escherichia coli* (BL21, DE3) and purified by affinity chromatography to at least 90% purity at Sanofi (Vitry-Sur-Seine).

### Evaluation of affinity and antagonistic properties of compounds with $His_6$-ERα-LBD proteins

Affinity was assessed by measuring the dissociation constant ($K_d$) using LanthaScreen TR-FRET ERα competitive binding assay; antagonistic properties were assessed by measuring the half maximal effective concentration ($EC_{50}$) using LanthaScreen TR-FRET ERα competitive binding assay. The antagonistic potency of the compounds was measured using a modified LanthaScreen TR-FRET ERα coactivator binding assay. All assays were from Thermo Fisher Scientific and were performed according to the manufacturer's instructions with modifications (see Supplementary Materials and Methods).

### Murine uterotrophic assay

Female bi-ovariectomized ICR mice aged 6 weeks were purchased from Taconic. Animals were used at least 10 days after bi-ovariectomy and randomized into groups ($n = 5$) and treated once-a-day 4 days with compounds of interest at indicated doses. Animals were euthanized 24 hours post the last dose and uteri were dissected, weighed and fixed in 10% neutral buffered formalin for histologic examination. A small portion of tissue was saved prior to fixation for mRNA isolation and gene expression analysis.

Formalin-fixed uteri samples were processed for paraffin embedding, sectioned at approximately 5 μm, and stained with hematoxylin and eosin. Endometrial layer thickness was measured using whole slide images obtained from digital scans using the Aperio AT slide scanner (Leica Biosystems) at 20× magnification. Obliquely sectioned areas were avoided. For each treatment group, uterus samples from five mice were examined. For each mouse, digital measurements were taken from three separate sections. Results are displayed as the mean endometrial layer thickness ± SE.

### Transcriptional reporter assays

The ligand binding domain of ERα (amino acids 246–595, NM_00125) or ERβ (amino acids 261–500, NM_001437) were synthesized by DNA 2.0 and was fused to the DNA binding domain of GAL4 in a doxycycline inducible plasmid (pCDNA5/FRT), which was stably integrated into HEK293 cells. These cells also stably express a luciferase reporter gene under the transcriptional control of the upstream activator sequence (PGL4.15luc2P/Hygro). These cell lines were maintained in DMEM supplemented with 10% FBS, 1 mg/mL blasticidin, 400 μg/mL Geneticin, and 50 μg/mL of Hygromycin (Thermo Fisher Scientific). A cell suspension containing 5,000 cells in phenol red free DMEM containing 5% CSS was transferred into a 384-well black-walled clear bottom tissue culture-coated plate. The microplates were incubated at 37°C and 5% $CO_2$ overnight. The following day, 3 hours prior to compound treatment, cells were stimulated by adding 0.5 μg/mL doxycycline (Clonetech) to induce NR-LBD expression. For agonist assays, the compounds were serially diluted and compound in DMEM supplemented with 5% CSS was added to the cells. For antagonist assays, the compounds were treated in DMEM with 5% CSS and 2 nmol/L of estradiol. After overnight incubation with the compound, luciferase reagent (Promega) was added to each well and the luminescence emitted was measured using an Envision Multilabel Reader (Perkin Elmer).

### RNA isolation and qPCR

RNA was extracted using the RNeasy Kit (Qiagen) per the manufacturers instruction, quantified by NanoDrop 8000 (Thermo Fisher Scientific) and reverse-transcribed with cDNA Archive Kit (Applied Biosystems). Taqman gene expression assays (Applied Biosystems) were used to quantify *PGR* (Hs00172183_m1), *Bcas1* (Hs00952822_m1), *CXCL12* (Hs03676656_mH), *BLNK1* (Hs00929914_m1), *IL20* (Hs00218888_m1), and the house-keeping genes PGK (Hs00391480_m1) and GAPDH (Hs99999905_m1) The relative quantities were determined using ΔΔ threshold cycle (ΔΔCt), according to the manufacturer's instructions (Applied Biosystems).

### RNA sequencing

RNA was extracted using the RNeasy Kit (Qiagen). The concentration of RNA samples was determined using NanoDrop 8000 (Thermo Fisher Scientific) and the integrity of RNA was determined by 4200 TapeStation (Agilent Technologies). RNA sequencing FASTQ files were processed with STAR aligner and Cufflinks to generate gene-level estimation of expression in transcripts per million (42, 43). The transcripts per million data were then quantile-normalized and $\log_2$-transformed. To identify genes that are differentially expressed between SERD compound treatment and DMSO (control) treatment groups, a two-factor (treatment and dose) ANOVA model was used at respective dose and time points. The treatment factor was fixed, with seven levels: six SERD compounds and the DMSO control. The dose factor was also fixed, with two levels: low and high. All samples were treated at 24 hours. *Post hoc* contrast analyses were performed at each dose and time level, between each SERD compound treatment and the DMSO control. Cut-off levels of absolute fold-change ≥1.5 and FDR-adjusted $P$-value ≤ 0.05 were used to select differentially expressed genes (DEG), which resulted in a panel of 1022 DEGs. This analysis was performed using Array Studio (Qiagen).

The panel of 1,022 genes identified as differentially expressed in at least one compound-versus-DMSO comparison were used for hierarchical clustering of compound treatment data normalized to DMSO control at respective dose and time points. Complete-linkage clustering was performed on the basis of Pearson correlation coefficients. Expression profile similarity between compounds was assessed by Pearson correlation on the DEGs.

### Pharmacokinetic and efficacy studies

HCI013 tumor fragments, MCF7, or MCF7 ERα-Y537S cell suspensions were implanted subcutaneously on the right flank of 6–8-week-old female athymic nude mice purchased from Envigo. HCI013 and MCF7 xenografts were supplemented subcutaneously with estradiol pellets (90-day release, 0.5 mg/pellet) to stimulate tumor growth. Tumors were measured in two dimensions twice weekly. Tumor volume was calculated by the formula: volume = length × (width [2])/2. When tumors reached an average size of roughly 150 to 350 $mm^3$, animals were randomized into groups and treatment was started. SAR439859 was formulated in 20% Labrasol 5% Solutol HS15 75% of 5% Dextrose at pH 5.5. Animals were sacrificed after the final dose and tumors were excised, cut into approximately 30 mg fragments and flash frozen for RNA and protein pharmacodynamic analysis. Additional tumor fragments for IHC were placed in 10% neutral buffered formalin for 24 hours

and transferred to 70% ethanol until processing. Sections (5 μm) were labeled for ERα (clone SP1, 790–4325 Ventana Roche) stained with Horseradish Peroxidase/3,3′-Diaminobenzidine Detection Kit (Abcam, #64261). Details of the FES/PET-CT imaging of the MCF7 xenograft tumors are provided in the Supplementary Materials and Methods.

## Results

### Identification and validation of SAR439859 as a novel SERD

To identify a nonsteroidal SERD with improved antitumor activity and oral bioavailability, we performed a high-throughput screening with the MCF7 breast cancer cell line using an in-cell Western immunofluorescence assay. Prospective optimization of the ER degradation and ERα antagonism structural motifs led to the identification of SAR439859 (**Fig. 1A**). The molecule is characterized by a fluoropropyl pyrrolidinyl side chain that is molecularly distinct from other SERD molecules. Treatment with SAR439859, like fulvestrant, leads to a strong reduction of both cytoplasmic and nuclear ERα compared with selective ERα modulators (SERM, **Fig. 1B**).

SAR439859 effectively induced ERα degradation in MCF7 breast cancer cells at subnanomolar concentrations (half maximal inhibitory concentration [$DC_{50}$] of 0.2 nmol/L) with maximal degradation levels ($D_{max}$) of 98% (**Table 1**). Addition of the proteasome inhibitor MG132 fully blocked SAR439859-induced ERα degradation, as shown with fulvestrant-induced ERα degradation (Supplementary Fig. S1A). In MCF7 cells, SAR439859 also effectively antagonized estradiol (E2)-mediated transcriptional activation of an ERα luciferase reporter construct with nanomolar potency comparable to that of fulvestrant (**Table 1**). We examined the transcriptional activity of SAR439859 on other nuclear hormone receptors (NR) including ERβ, glucocorticoid receptor, androgen receptor, progesterone receptor, and mineralocorticoid receptor. SAR439859 was found to antagonize ERβ transcriptional activity (**Table 1**) but had no activity against other NRs at concentrations up to 5 μmol/L.

To further confirm the selective antagonistic effect of SAR439859 on ERα signaling, we evaluated the impact of SAR439859 on the expression of well-described ER target genes in MCF7 cells (26, 44–46). Both SAR439859 and fulvestrant showed similar patterns of down-modulation of gene expression of the ERα target gene panel and was differentiated from the partial agonism induced by tamoxifen. (**Fig. 1C**).

SAR439859 potently inhibited the proliferation of MCF7 cells (Supplementary Fig. S1B) but had no effect on the growth of ER-negative cell lines even at the highest concentration tested (5 μmol/L) confirming the high selectivity of SAR439859 for ERα-dependent tumor cells. In a tamoxifen-resistant MCF7 derived model, LCC2, SAR439859 inhibited the growth with an $IC_{50}$ of 16 nmol/L indicating that the compound is not cross-resistant with tamoxifen (**Fig. 1D**; ref. 47).

ERα mutations with gain-of-function capabilities have shown to be one of the resistance mechanisms against anti-ERα therapies in patients with breast cancer (10). We therefore assessed SAR439859 activity against wild-type (WT) and mutant ERα on recombinant ERα LBD proteins. Unlike the ERα WT receptor, Y537S and D538G mutations in the ERα LBD lead to spontaneous recruitment of coactivators, such as the peroxisome proliferator-activated receptor-γ coactivator and the steroid receptor coactivators, in the absence of estradiol (**Fig. 1E**; Supplementary Fig. S2), confirming that these mutations cause constitutive activation of ERα (17). In this activated conformation, mutant ERα receptors have increased affinity for the agonist, E2, and decreased affinity for the antagonists, including SAR439859, as illustrated by the corresponding changes in $K_d$ values (**Fig. 1F**; Supplementary Fig. S3; Supplementary Table S1). Therefore, SAR439859 antagonizes mutant ERα with lower potency than WT ERα [$EC_{50}$ values were determined in the presence of 10 nmol/L estradiol: 20 nmol/L (WT), 331 nmol/L (Y537S mutant), 595 nmol/L (D538G mutant); **Fig. 1G**; Supplementary Table S1]. To understand the effect of these mutations in the cellular context, MCF7 cells were engineered to express WT or mutant ERα under a doxycycline-inducible promoter. Interestingly, the doxycycline-induced expression of mutant but not WT ERα led to constitutive expression of the ERα target genes *CXCL12, PGR*, and *GREB1* (Supplementary Fig. S1C). In these engineered MCF7 cell lines, both SAR439859 and fulvestrant treatment dose-dependently inhibited *CXCL12* and *PGR* and increased *Bcas1* expression in both mutants and WT ER cells (Supplementary Fig. S4). Furthermore, SAR439859, like fulvestrant, was able to downregulate both WT and HA-tagged Y537S and D538G mutant ERα protein levels (**Fig. 1H**). In the absence of E2, SAR439859 inhibited growth in a dose-dependent manner in MCF7 cells over-expressing WT, Y537S, or D538G ERα, with a 2- to 10-fold reduction in potency in ERα mutant compared with ERα WT cells ($IC_{50}$ of 0.4, 10, and 1 nmol/L, respectively; **Fig. 1I**). This trend in reduced potency against ERα mutants was consistent for both fulvestrant (**Fig. 1J**) and tamoxifen (**Table 1**).

### SAR439859 has no agonist activity in murine uterotrophic assay

Consistent with published data, oral administration of tamoxifen 30 mg/kg daily significantly increased uterine wet weight. In contrast, SAR439859 at doses of 25, 50, and 100 mg/kg daily, and fulvestrant dosed at 100 mg/kg subcutaneously every other day, had no statistically significant effect on uterine wet weight (**Fig. 2A**). Histologic staining of SAR439859-treated uterine tissue samples showed that both endometrial cell thickness and epithelial height were not affected compared with control samples (**Fig. 2B**, **C**, and **E**). In addition, ERα target gene expression of C3-complement was increased in tamoxifen treated mice but it was unchanged in mice treated with fulvestrant or SAR439859 (**Fig. 2D**), confirming that SAR439859 does not have agonist activity in uterine tissue.

### Pharmacodynamic response and antitumor activity of SAR439859

We next assessed SAR439859 *in vivo* antitumor activity using MCF7 cell xenograft mouse models overexpressing either WT (ERα-WT) or mutant Y537S ER (ERα -Y537S). The overexpression of WT ERα conferred estrogen-dependent tumor growth, whereas the doxycycline-inducible overexpression of Y537S ERα resulted in estrogen-independent tumor growth (Supplementary Figs. S5A and S5B). Pharmacokinetic analysis of the ERα-Y537S mice that were administered with SAR439859 showed a dose-proportional increase in tumor exposure with an AUC from time zero to last measurable concentration ($AUC_{last}$) of 21,300 ng·h/mL and maximum concentration of 2,280 ng/mL at the 25 mg/kg dose (**Fig. 3A**; Supplementary Table S2). SAR439859 displayed a moderate clearance of 1.92 L/h·kg and 62.2% oral bioavailability following administration of a 25 mg/kg dose. It was noteworthy that the apparent volume of distribution at steady state was large, calculated at 6.1 L, resulting in an AUC tumor/plasma ratio of 1.2 (Supplementary Table S2).

In terms of efficacy, SAR439859 induced dose-dependent inhibition of ERα-WT and ERα-Y537S tumor growth, with tumor regression achieved at doses of 12.5 and 25 mg/kg (–5 and –28 and –9 and –34 Δtumor/Δcontrol, respectively; Supplementary Fig. S5C; **Fig. 3B**;

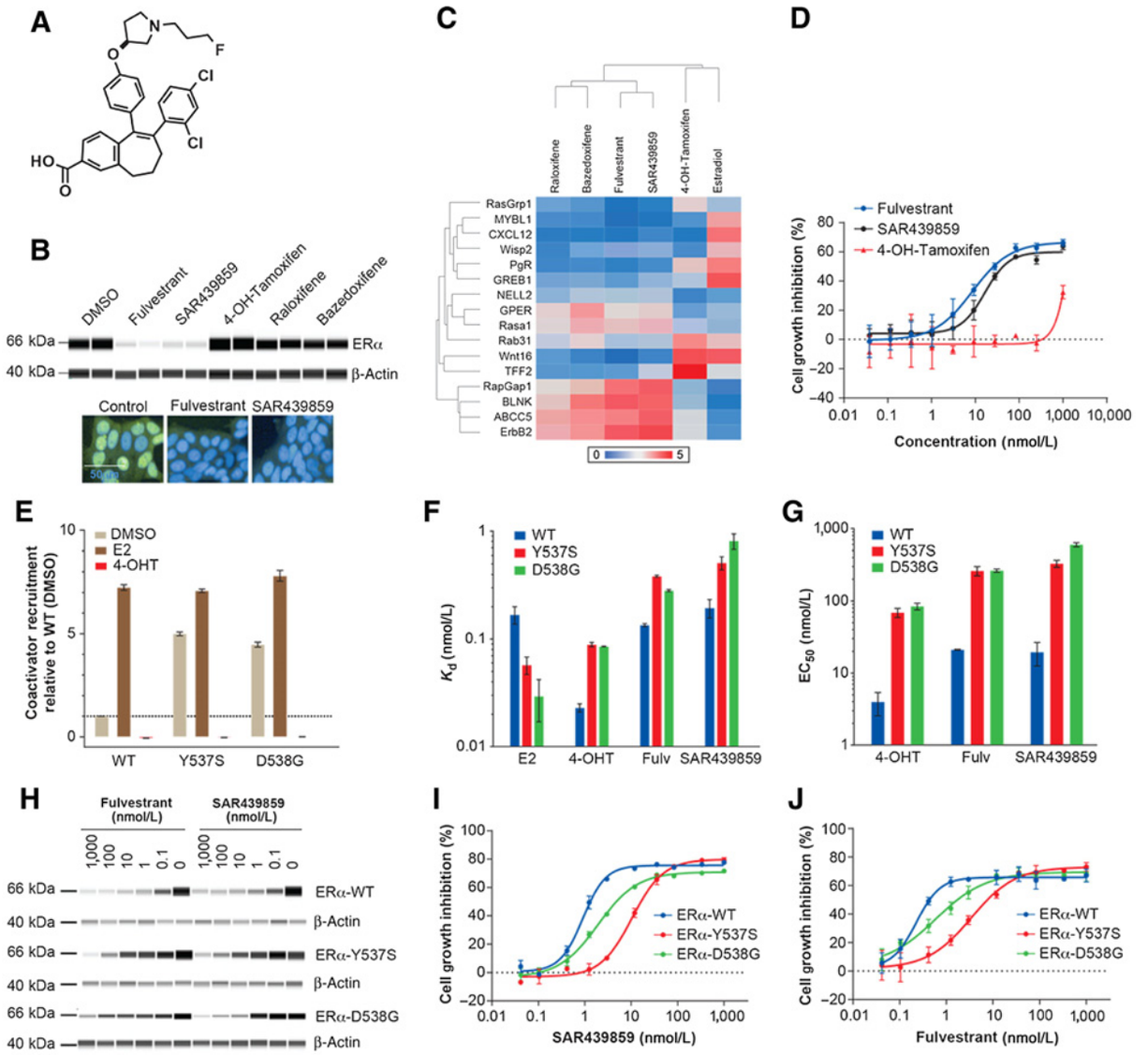


**Figure 1.**

SAR439859 is a potent antagonist and degrader of mutant and WT ER. **A,** SAR439859 structure. **B,** Simple Western analysis of the effect of SAR439859, fulvestrant, bazedoxifene, 4-hydroxytamoxifen, and raloxifene on the ERα protein level in MCF7 cells (4 hours post-300 nmol/L compound treatment, in biological duplicates). **C,** Transcriptional activity of benchmark ERα ligands in MCF7 cells. Transcriptional activity was monitored using a selective ER modulator discriminatory target gene set following 24-hour 300 nmol/L ligand treatment. Data were $\log_2$ normalized followed by standardization and hierarchical clustering; **D,** LCC2 cell viability assay comparing SAR439859 with fulvestrant, bazedoxifene, 4-OHT, and raloxifene after 7 days of treatment. **E,** Coactivator peptide recruitment by the WT and mutant $His_6$-ERα-LBD measured in the presence of either DMSO, estradiol (E2), or 4-OHT; all values were normalized by the value obtained for the WT $His_6$-ERα-LBD in the presence of DMSO. Data represent mean and SD for six replicates. **F,** Compound affinity for the WT and mutant recombinant His6-ERα-LBD proteins. Data represent mean and range for values obtained in two independent experiments, each conducted with at least two replicates. **G,** Antagonistic potency of compounds measured with recombinant $His_6$-ERα-LBD proteins in the presence of 10 nmol/L estradiol. Data represent mean and range for values obtained in two independent experiments, each conducted with at least three replicates. **H,** Simple Western analysis of ERα protein level comparing SAR439859 with fulvestrant in dose response 4-hour post-compound treatment in MCF7 cells with overexpression of WT, mutant Y537S or D538G ERα. **I, J,** Cell viability assay comparing SAR439859 or fulvestrant activity, respectively, in MCF7 cells with overexpression of WT, mutant Y537S or D538G. Cell growth inhibition is presented as a percentage of CellTiterGlo activity relative to the vehicle control after 10-days compound incubation. Data represent mean and SD for three replicates. 4-OHT, 4-OH-tamoxifen.

Supplementary Table S3). Consistent with the observed antitumor activity, Simple Western blotting revealed a dose-dependent reduction in total ERα protein levels in the ERα-Y537S xenograft tumors following treatment with SAR439859 (**Fig. 3C**). SAR439859 also demonstrated a time- and dose-dependent modulation of ERα target gene expression, leading to inhibition of *IL20*, *PGR* and *CXCL12* gene expression as well as an increase in *Blnk* and *Bcas1* gene expression. (**Fig. 3D–F**; ref. 48).

**Table 1.** SAR439859 *in vitro* properties.

| Assay description | ERα transcription luciferase | ERβ transcription luciferase | MCF7 ERα degradation | | MCF7 cell viability | | MCF7 (*Y537S*) cell viability | | MCF7 (*D538G*) cell viability | |
|---|---|---|---|---|---|---|---|---|---|---|
| **Compounds** | **$IC_{50}$ (nmol/L)** | **$IC_{50}$ (nmol/L)** | **$DC_{50}$ (nmol/L)** | **$D_{max}$ (%)** | **$IC_{50}$ (nmol/L)** | **$E_{max}$ (%)** | **$IC_{50}$ (nmol/L)** | **$E_{max}$ (%)** | **$IC_{50}$ (nmol/L)** | **$E_{max}$ (%)** |
| SAR439859 | 1.8 | 8.4 | 0.4 | 98 | 1.1 | 64 | 10.0 | 79.8 | 1.0 | 70.1 |
| 4-OH-Tamoxifen | 0.9 | 0.5 | NA | NA | 4.2 | 53 | 20.1 | 61.4 | 6.5 | 51.8 |
| Fulvestrant | 0.5 | 0.9 | 0.2 | 98 | 0.3 | 65 | 2.9 | 76.7 | 0.65 | 68.1 |

Abbreviation: NA, not applicable.

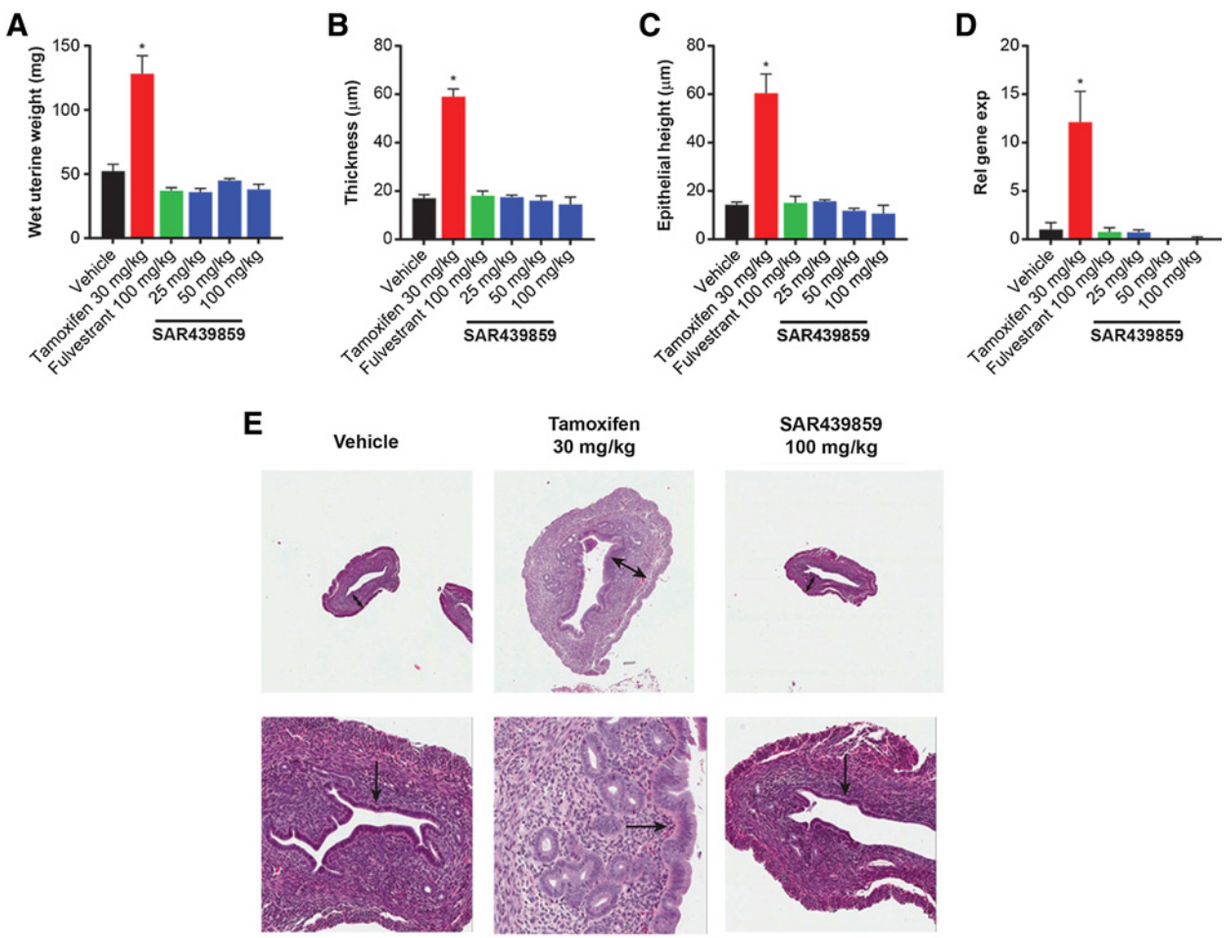


**Figure 2.**

Effect of SAR439859 on uterine tissue. **A,** Wet uterine weight measurements from bi-ovariectomized juvenile mice treated with specified ERα ligands for 5 days. 4-OHT and fulvestrant were treated as controls. Endometrial thickness (**B**) and epithelial height (**C**) were digitally measured using whole slide images of hematoxylin and eosin stained cross-sections of uteri. For each mouse, three cross-sections were analyzed (five mice per group). Results are displayed as the mean endometrial thickness from animals ± deviation ($n = 3$). **D,** C3-complement gene expression was assessed by RT-qPCR reach after treatment with indicated compounds. **E,** Photomicrographs of uterine cross-sections showing endometrium layer (double-headed arrows) and luminal epithelial cell height (single-head arrows). *, denotes significance ($P < 0.001$) compared with vehicle in an unpaired *t* test for **A, B, C,** and **D**.

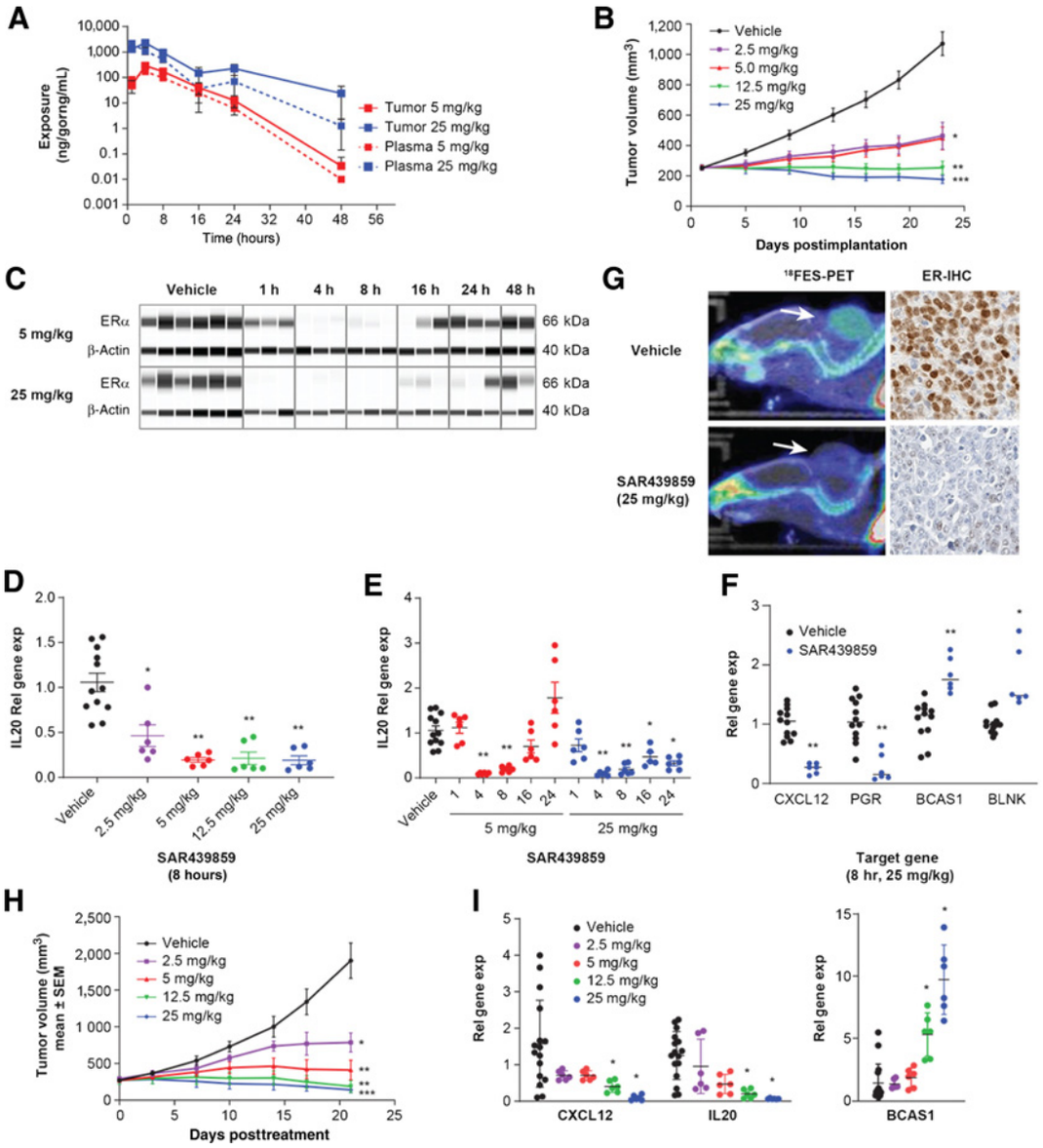


**Figure 3.**

Pharmacokinetic/pharmacodynamic relationship and antitumor activity of SAR439859. MCF7 ER Y537S overexpressing tumors were implanted in animals without supplemental 17β-estradiol pellets. **A,** Plasma (ng/mL) and tumor (ng/g) exposure of SAR439859 post–single-dose administration at indicated time. Tumors were harvested for ERα protein and ERα target gene transcription assessment. **B,** Mean tumor volume over time in mouse xenograft dosed with vehicle or SAR439859 2.5, 5, 12.5, or 25 mg/kg (twice daily, orally). Tumor volume was evaluated twice per week until the study endpoint. **C,** Simple Western analysis of ERα level in tumors from **A** collected after SAR439859 dose at indicated time with each lane representing an individual tumor sample. **D–F,** Gene expression analysis of tumors from **A** in mice treated with SAR439859 compared with vehicle at time indicated with each point representing individual tumor sample. **D,** Dose-dependent effect on *IL20* expression. **E,** Time-dependent effect on *IL20* expression after 5 or 25 mg/kg SAR439859 dosing; **F,** Inhibition of *CXCL12* and *PGR* expression and induction of Bcas1 and Blnk1 expression after 8 hours; unpaired t test: *, $P < 0.05$; **, $P < 0.001$ versus vehicle for **D–F**. **G,** Representative $^{18}$F-FES-PET (left) and IHC images (right) of MCF7 ER Y537S tumors treated with either vehicle or SAR439859 and probed using anti- ERα antibody. $^{18}$F-FES-PET images were taken 4 hours after administration of SAR439859. **H**, Mean tumor volume over time in mice with the HCI013 xenograft model treated with SAR439859. Significance at end of study was determined by unpaired *t* test: *, $P < 0.001$; **, $P < 0.01$; ***, $P < 0.05$ compared with vehicle, 2.5 and 5 mg/kg SAR439859. **I,** Gene expression in the HCI013 model treated with SAR439859. *, $P < 0.05$ versus vehicle using unpaired *t* test.

In an effort to validate an additional clinically-relevant target engagement biomarker, tumor ERα occupancy was monitored by PET using $^{18}$F-fluoroestradiol (FES) uptake (49). $^{18}$F-FES-PET imaging was carried out on mice bearing ERα-Y537S xenograft tumors following SAR439859 treatment (25 mg/kg twice daily). After compound administration, the $^{18}$F-FES-PET signal was decreased by approximately 75% compared with control (**Fig. 3G**). IHC analysis of tumor samples confirmed downregulation in ERα protein levels that could contribute to the decrease in $^{18}$F-FES-PET signal induced by SAR439859 (**Fig. 3G**).

We further evaluated SAR439859 antitumor activity in HCI013, a patient-derived xenograft (PDX) model that harbors the Y537S *ESR1* mutation. The original tumor was obtained from a patient with ERα + metastatic breast cancer who relapsed on several lines of hormonal therapy, including tamoxifen (37, 50, 51). Mouse models bearing the HCI013 PDX and treated orally with SAR439859 (2.5–25 mg/kg twice daily) had a dose-dependent inhibition of tumor growth. Statistically significant tumor regressions were achieved at doses of 12.5 and 25 mg/kg (–31 and –46 Δtumor/Δcontrol; **Fig. 3H**; Supplementary Table S3). Sustained tumor growth regression was observed even 3 weeks after SAR439859 treatment was discontinued (Supplementary Fig. S5D). In agreement with its antitumor activity, SAR439859 also induced dose-dependent and sustained modulation of ERα target genes. Notably, *CXCL12* and *IL20* expression were decreased, whereas *Bcas1* expression was significantly increased at 8 hours posttreatment (**Fig. 3I**).

### Fluoroalkylamine side chain of SAR439859 improves ERα degradation across breast cancer cell lines

To delineate the relationship between ERα degradation and SERD antitumor activity, we evaluated ERα degradation in a panel of 14 ERα + breast cancer cell lines and compared the effect of SAR439859 with other SERDs including GDC-0810, AZD9496, and fulvestrant (**Fig. 4A**). ERα protein levels were normalized against β-actin and % residual ER abundance is reported in Supplementary Table S4, for all compounds shown in **Fig. 4B**. In the MCF7 cells, all SERD compounds induced ERα degradation, whereas differential ERα protein levels were observed across the other cell lines tested (**Fig. 4B**). Specifically, GDC-0810 or AZD9496 induced partial or weak ERα degradation, whereas SAR439859 and fulvestrant efficiently degraded the ERα in the cell lines assessed (**Fig. 4B**). This trend was mirrored in immunofluorescence image analyses of nuclear and cytoplasmic ERα in MDAMB134VI and SUM44PE cells (**Fig. 4C**).

To elucidate the role of the SERD side chains, we exchanged the cinnamic acid side chain in the GDC-0810 and AZD-9496 molecules with the amine side chain from the SAR439859 molecule, which resulted in new hybrid molecules designated as GDC-SAR and AZD-SAR, respectively (WO2018091153; **Fig. 4A**). The ability to potently bind and inhibit the ER was preserved in these hybrid molecules (Supplementary Table S1). Strikingly, GDC-SAR and AZD-SAR demonstrated a marked increase in ER degradation compared with their respective parent compounds and showed an ERα degradation profile more comparable to that of SAR439859 or fulvestrant across the majority of ERα+ breast cancer cell-lines assessed (**Fig. 4B**; Supplementary Table S4).

To unmask the ER-intrinsic activity, we then evaluated gene expression after compound treatment in HCC1428-LTED cells, which is a cell line that is hormone-deprived. Changes in global mRNA expression were assessed 24 hours posttreatment. Hierarchical clustering on a selected panel of 1,022 transcripts identified two groups with differing signatures: one group included GDC-0810 and AZD9496, and the other group included fulvestrant, SAR439859, GDC-SAR, and AZD-SAR (**Fig. 4D**; Supplementary Excel File). Statistical correlation revealed that the SAR439859-induced expression profile is closely correlated to fulvestrant. However, GDC-0810 and AZD9496 transcript profiles only weakly correlated to that of fulvestrant. Interestingly, the profiles of the hybrid molecules GDC-SAR and AZD-SAR, are also closely correlated to those of fulvestrant and SAR439859 (**Fig. 4D**; Supplementary Fig. S6).

To assess the relative ER modulating activity of the compounds, an ER Signature (87 genes, Supplementary Excel File) was developed by transcriptional profiling of multiple cell lines to identify genes that were modulated by estradiol and then blocked by SERM and SERD. An ER Activity Score was then assessed using gene set variation analysis (GSVA) on the ER Signature (52). Fulvestrant and SAR439859 demonstrated a deep inhibition of ER activity, whereas GDC-0810 and AZD9496 only partially inhibited ERα activity further supporting the above observations. Interestingly, both hybrid molecules, GDC-SAR and AZD-SAR, also strongly inhibited ERα transcriptional activity (**Fig. 4E**). Gene expression analysis provided further confirmation of the differential response of these molecules on well-validated ERα target genes (26, 46). SAR439859, GDC-SAR, and AZD-SAR inhibited expression of *CXCL12* and induced expression of *Bcas1*, whereas GDC-0810 and AZD9496 failed to elicit any significant change in the expression of these genes (**Fig. 4F**). Remarkably, SAR439859 and fulvestrant induced a profound modulation of ERα intrinsic activity in the absence of E2, suggesting a strong inverse agonist activity of these compounds.

### Improved ERα degradation and ERα transcriptional inhibition of SAR439859 leads to more effective *in vitro* and *in vivo* antitumor activity

All SERDs demonstrated similar effective inhibition of MCF7 cell growth ($E_{max}$; approximately 60% growth inhibition observed after 10 days of treatment) despite varying levels of potency ($IC_{50}$ range: 0.3–20 nmol/L; **Fig. 5A**). However, in the MDAMB134VI cell line, GDC-0810 and AZD9496 induced only a partial growth inhibition compared with SAR439859 ($E_{max}$ of 20% vs. 60%; **Fig. 5B**). These findings were recapitulated in other breast cancer cell lines, including HCC1428-LTED, SUM44PE, HCC1500, and HCC1428 (**Fig. 5C**). GDC-SAR and AZD-SAR also exhibited greater growth inhibition compared with GDC-0810 or AZD9496, underlining the importance of specific structural elements in driving mechanistic and functional divergence between SERD compounds.

We wanted to confirm that HCI013 was a suitable *in vivo* model that would discriminate the differential effect of these molecules on tumor growth. To this end, fresh, viable HCI013 tumor tissue was dissociated and cultured *ex vivo* before being treated with saturating concentrations of the SERD compounds for 24 hours. Compared with GDC-0810 and AZD9496, SAR439859 and fulvestrant exhibited stronger ERα degradation and greater inhibition of *CXCL12* gene expression (**Fig. 5D** and **E**).

Consequently, the antitumor activity of tamoxifen, fulvestrant, SAR439859, and GDC-0180 was examined *in vivo* in the HCI013 model. As expected, tamoxifen administered at 30 mg/kg every day did not inhibit tumor growth (**Fig. 5F**). The analysis of the pharmacodynamic effect in HCI013 tumors collected after tamoxifen treatment showed increased ER protein levels and induced the expression of *PGR* which is normally repressed by ER antagonist or degrader compounds (**Fig. 5G**), suggesting that the agonist activity of tamoxifen could account for the resistance of the HCI013 tumor model to this ligand class. Despite its strong *in vitro* antiproliferative activity, fulvestrant at 200 mg/kg twice weekly induced only a partial *in vivo* antitumor activity in the HCI013 model (**Fig. 5F**; Supplementary Figs. S7A–S7C) consistent with previous reports (26, 28, 35).

Interestingly, SAR439859 showed a superior antitumor activity, inducing tumor regression (Δtumor/Δcontrol of −34%) at 100 mg/kg every day, compared with the partial antitumor activity (Δtumor/

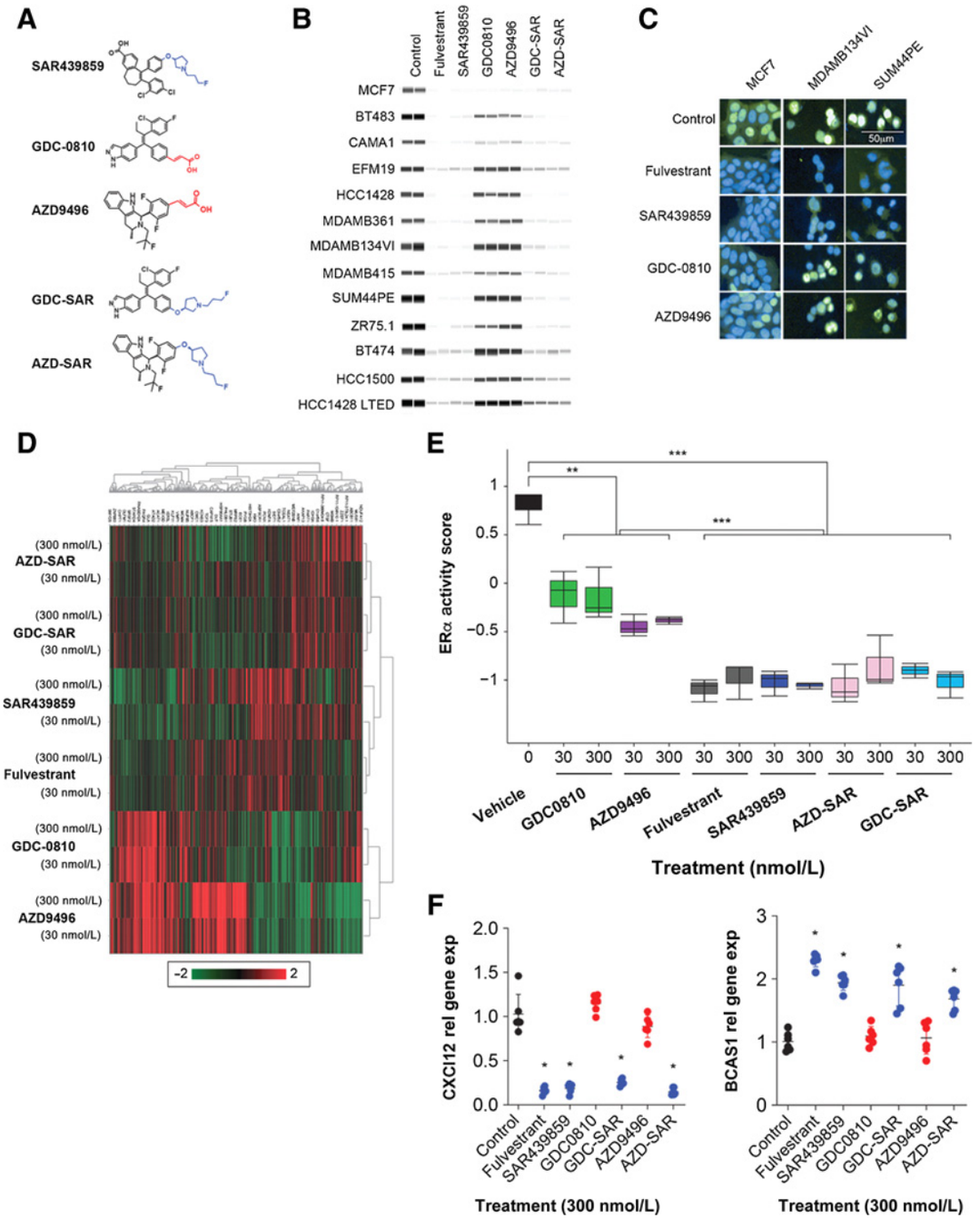


**Figure 4.**

Differential effect of fluoropropyl-pyrrolidinyl amine versus cinnamic acid side chains on ER degradation and gene expression. **A,** Structures of SAR439859, GDC-0810, AZD9496, and the hybrid molecules GDC-SAR and AZD-SAR; cinnamic acid side chains are shown in red, and fluoropropyl-pyrrolidinyl amine side chains are shown in blue. **B,** ERα Simple Western comparing SAR439859 with fulvestrant, GDC-0810, AZD9496, GDC-SAR, and AZD-SAR 4 hours post-300 nmol/L compound treatment in duplicate in 14 breast cancer cell lines. Residual ER (%) was normalized against β-actin and can be found in Supplementary Table S4. **C,** Representative images of ERα In-Cell Western immunofluorescence assay comparing SAR439859 with fulvestrant, GDC-0810, and AZD9496 in three breast cancer cell lines. **D,** Heatmap of 1,022 genes differentially expressed in the HCC1428 LTED breast cancer cell line in absence of exogenous estrogen at two doses (30 and 300 nmol/L). Data were $\log_2$ normalized followed by standardization and hierarchical clustering. **E,** ER transcriptional activity using ER signature and expressed as ER activity score from GSVA; Wilcoxon test is used to compare the means of delineated groups with **, $P < 0.01$ and ***, $P < 0.001$. **F,** RT-qPCR analysis of the effect of the different selective ER degrader molecules on the expression of ERα target genes *CXCL12* and Bcas1. *, Denotes significance ($P < 0.01$) compared with unpaired *t* test.

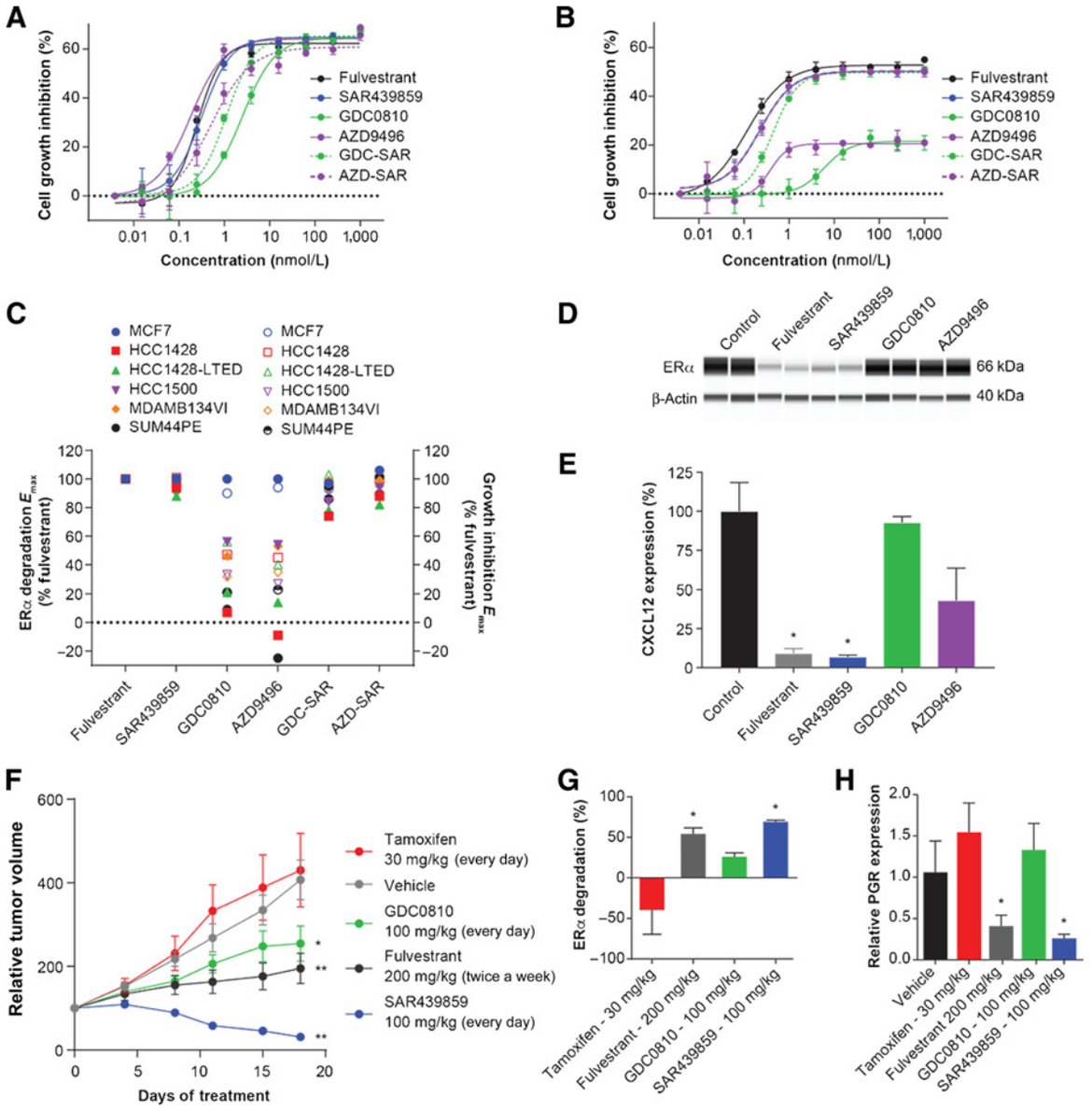


**Figure 5.**

SERDs with fluoropropyl-pyrrolidinyl amine side chain show improved ER degradation, antiproliferative, and antitumor efficacy *in vitro* and *in vivo*. Effect of SERD molecules on cell viability in MCF7 (**A**) and MDAMB134VI (**B**) cells. Compound treatment was for 10 days. **C,** Comparison of the maximum percentage of ERα degradation (solid shapes) with the maximum percentage growth inhibition (open shapes) in six breast cancer cell lines. Cell viability is expressed as relative percentage compared with fulvestrant treatment. Simple Western ERα protein level (**D**) and RT-qPCR analysis (**E**) in *ex vivo* HCI013 breast cancer human xenograft that have been dissociated and maintained *in vitro* before being treated with SERD molecules for 24 hours. Error bars represent the SD from the mean from biological triplicates. **F,** Effect of different ERα ligands on the tumor growth of the HCI013 breast cancer human xenograft model. *, $P < 0.05$; **, $P < 0.001$ denotes significance compared with vehicle treated group at end of study using unpaired *t* test. **G,** Quantification of ERα protein levels in tumor samples of four individual mice normalized to β-actin. **H,** Analysis of *PGR* gene expression in tumors collected after last administration at 8 hours. **D, E, H,** *, $P < 0.05$ denotes significance compared with vehicle treated group at end of study using unpaired *t* test.

Δcontrol of 27%) achieved by GDC-0810 at 100 mg/kg every day (**Fig. 5F**). These results are in line with the superior antiproliferative activity of SAR439859 compared with GDC-0810 observed *in vitro* in breast cancer cell lines. To assess the pharmacodynamic effect on the ERα pathway, ERα protein was analyzed in HCI013 tumors after treatment with the two SERD compounds. SAR439859 induced greater ERα degradation than GDC-0810 (approximately 80% vs. 30% decrease in the ERα, respectively; **Fig. 5H**).

RT-qPCR analysis of individual ERα repressed genes such as *PGR* and *CXCL12* confirmed stronger inhibition by SAR439859 compared with fulvestrant or GDC-0810 in HCI013 tumors (**Fig. 5H**; Supplementary Fig. S8A, respectively). We then analyzed

the ERα transcriptional activity in the HCI013 model using the panel of genes corresponding to the ER gene signature derived from our *in vitro* cell line analysis as described previously. Both SAR439859 and GDC-0810 treatments displayed suppressive activity of ERα signaling, with more marked ERα suppression achieved by SAR439859 compared with GDC-0810 (Supplementary Fig. S8B).

## Discussion

Identification of a novel, best-in-class SERD has been a major focus of research and drug development for the treatment of ER+ breast cancer. SAR439859 is a novel SERD that has a biological profile and pharmacokinetic properties that distinguish it from other SERMs and SERDs that have entered the clinic. SAR439859 did not exhibit ERα agonistic activity when compared with tamoxifen on the uterus. At 100 mg/kg dose, which achieves tumor growth inhibition in tumor models, no increase in uterine wet weight, endometrial thickness or C3-complement gene expression was observed suggesting that SAR439859 is inducing ERα full antagonist activity (**Fig. 2A–D**). These biological observations are in agreement with SAR439859 inducing conformational change in helix 12 of the ERα (53).

As mechanisms of resistance to endocrine therapy continue to emerge, it is important to understand the efficacy of these ligands on both WT and mutant ERs in breast cancer models. SAR439859 is a nonsteroidal, potent, full antagonist with high affinity for ERα and degrades the WT and mutant Y537S and D538G ER, suggesting that these mutations do not preclude SAR439859-induced ERα degradation (**Fig. 1**). Potent antagonist and anti-proliferative activity were observed *in vitro* in MCF7 driven by either WT or mutant ERα, as well as tamoxifen resistant LCC2 breast cancer cells (**Fig. 1D** and **I**; Supplementary Fig. S1B). This anti-proliferative activity on MCF7 and Y537S ER MCF7 translated to tumor regression in these *in vivo* xenograft models (**Fig. 3B**; Supplementary Fig. S3C). Furthermore, SAR439859 demonstrated antitumor activity in HCI013 PDX, which harbors the Y537S mutation and is resistant to tamoxifen treatment (Supplementary Table S3; **Fig. 3H**; Supplementary Fig. S4D). These results suggest that SAR439859 may be an effective therapy to combat resistance induced by tamoxifen treatment or by the development of ER LBD mutations.

In this study we show that SAR439859, with its fluoropropyl-pyrrolidinyl side chain, displays a differential biology compared with SERDs containing a cinnamic acid side chain, such as GDC-0810 and AZD9496. Indeed, SAR439859 displayed greater ERα signaling suppression and higher ERα degradation ($D_{max}$), that was positively correlated to maximal growth inhibition ($E_{max}$) across many breast cancer cell lines.

Replacement of the cinnamic side chain in the GDC-0810 or AZD9496 molecules with fluoropropyl pyrrolidinyl side chain confirms the important role that this side chain has in SERD-mediated ERα antagonism and degradation. Indeed, both hybrid compounds, GDC-SAR and AZD-SAR, improved inhibition of ERα target gene expression as well as ERα degradation, compared with their parent compounds. In addition, the transcriptional signatures revealed that SERD molecules containing the fluoropropyl-pyrrolidinyl side chain cluster close to fulvestrant, suggesting a common mechanism of action. Furthermore, in the HCI013 PDX model, SAR439859 had improved efficacy over GDC-0810 and demonstrates antitumor activity achieving tumor regression at multiple doses (12.5 and 25 mg/kg; Supplementary Table S3; **Fig. 3H**). SAR439859 antitumor activity was correlated to a downregulation in ERα protein levels and an inhibition of ERα activity. Interestingly, several studies have reported that in in vivo MCF7 xenograft model, GDC-0810 at the selected dose of 100 mg/kg, like SAR439859 can drive complete ERα saturation and tumor regression (26, 35). These data are consistent with the aforementioned *in vitro* data and suggests that MCF7 model alone cannot discriminate between different classes of SERD compounds and therefore testing additional breast cancer models is critical to identify the SERD with optimal ERα antagonist and degrader activity.

In our study, cell lines with higher ERα protein levels such as MDA-MB-134VI, SUM44PE, and HCC1428-LTED exhibited the most functional divergence between the two classes of SERD compounds (Supplementary Fig. S9; Supplementary Table S4). In these cell lines, GDC-0810 and AZD9496 showed suboptimal antiproliferative activity, questioning the potential role of ERα protein levels in resistance to ERα-targeted therapies, such as SERDs containing cinnamic acid side chains. Consistent with our study, a recent report by Guan and colleagues also reported a functional divergence between the SERD classes defined by a fluoroalkylamine or cinnamic acid side chain, with improved ERα antagonism and degradation resulting in higher *in vitro* and *in vivo* efficacy of GDC-0927, a SERD containing a fluoroalkylamine side chain (26).

SAR439859 has a similar *in vitro* biological profile to fulvestrant with regards to ER antagonism, degradation, target gene signature and inhibition on tumor cell proliferation. However, SAR439859 achieves tumor regression in HCI013 PDX model whereas fulvestrant treatment at 200 mg/kg with exposure 8×-fold higher than the human equivalent dose, results in partial antitumor activity (**Fig 5F**; Supplementary Figs. S7A–S7C; refs. 20, 54). Importantly, SAR439859, unlike fulvestrant, can be administered orally and is not limited by its dose and exposure.

In summary, these results highlight the importance of specific structural elements in driving full ERα antagonism and maximal ERα degradation which achieves strong suppression of the ERα signaling pathway, induces greater growth inhibition across a broad range of breast cancer cell lines, and improves *in vivo* efficacy. On the basis of its global preclinical profile and *in vivo* anti-tumor activity, SAR439859 has key mechanistic features to become a best-in-class SERD with the potential to show broader clinical benefit than fulvestrant in patients post-tamoxifen treatment. SAR439859 is currently undergoing clinical trials to assess whether these preclinical observations can be confirmed in breast cancer patients. The outcomes from ongoing clinical trials assessing SAR439859 as a single agent and in combination with palbociclib (NCT03284957) in patients with ER+/HER2− metastatic breast cancer, who have previously received hormonal therapy, are being eagerly awaited.

## Data Availability

RNA-seq raw data, count matrix, and metadata are publicly available in the Gene Expression Omnibus (https://www.ncbi.nlm.nih.gov/geo/) under data repository accession no. GSE154058.

### Authors' Disclosures

J. Pollard reports personal fees from Sanofi during the conduct of the study, personal fees from Sanofi outside the submitted work, and a patent for SARD relationships pending. Y. El-Ahmad reports a patent for WO2017140669 issued. V. Certal reports a patent for WO2017140669 issued to Sanofi. B. Filoche-Rommé reports a patent for EP 16305174.1 issued. C. Garcia-Echeverria reports other disclosures from Sanofi outside the submitted work. M. Bouaboula reports nonfinancial support from Sanofi during the conduct of the study; nonfinancial support from Sanofi outside the submitted work; and a patent for the discovery of SAR439859 issued. No disclosures were reported by the other authors.

## Authors' Contributions

**M. Shomali:** Conceptualization, formal analysis, investigation, writing–original draft, writing–review and editing. **J. Cheng:** Investigation. **F. Sun:** Validation, investigation. **M. Koundinya:** Investigation, writing–review and editing. **Z. Guo:** Investigation. **A.T. Hebert:** Investigation. **J. McManus:** Investigation. **M.N. Levit:** Validation, investigation, writing–original draft. **D. Hoffmann:** Investigation. **A. Courjaud:** Investigation. **R. Arrebola:** Validation. **H. Cao:** Software, formal analysis. **J. Pollard:** Validation. **J.S. Lee:** Software, formal analysis. **L. Besret:** Investigation. **A. Caron:** Investigation. **D.S. Bangari:** Investigation. **P.-Y. Abecassis:** Formal analysis. **L. Schio:** Validation. **Y. El-Ahmad:** Investigation. **F. Halley:** Investigation. **M. Tabart:** Investigation. **V. Certal:** Investigation. **F. Thompson:** Investigation. **G. McCort:** Investigation. **B. Filoche-Romme:** Software. **H. Cheng:** Supervision. **C. Garcia-Echeverria:** Conceptualization, writing–original draft. **L. Debussche:** Supervision. **M. Bouaboula:** Conceptualization, supervision, writing–original draft.

## Acknowledgments

We would like to thank Carlos Arteaga for providing the HCC1428 LTED cells, Robert Clarke for providing the LCC2 cells, and Alana Welms for providing the HCI013 PDX models.

The costs of publication of this article were defrayed in part by the payment of page charges. This article must therefore be hereby marked *advertisement* in accordance with 18 U.S.C. Section 1734 solely to indicate this fact.

Received May 8, 2020; revised August 31, 2020; accepted November 3, 2020; published first December 11, 2020.

## References

1. Early Breast Cancer Trialists' Collaborative Group (EBCTCG), Davies C, Godwin J, Gray R, Clarke M, Cutter D, et al. Relevance of breast cancer hormone receptors and other factors to the efficacy of adjuvant tamoxifen: patient-level meta-analysis of randomised trials. Lancet 2011;378:771–84.
2. Cuzick J, Sestak I, Baum M, Buzdar A, Howell A, Dowsett M, et al. Effect of anastrozole and tamoxifen as adjuvant treatment for early-stage breast cancer: 10-year analysis of the ATAC trial. Lancet Oncol 2010;11:1135–41.
3. Aihara T, Yokota I, Hozumi Y, Aogi K, Iwata H, Tamura M, et al. Anastrozole versus tamoxifen as adjuvant therapy for Japanese postmenopausal patients with hormone-responsive breast cancer: efficacy results of long-term follow-up data from the N-SAS BC 03 trial. Breast Cancer Res Treat 2014;148:337–43.
4. Dowsett M, Cuzick J, Ingle J, Coates A, Forbes J, Bliss J, et al. Meta-analysis of breast cancer outcomes in adjuvant trials of aromatase inhibitors versus tamoxifen. J Clin Oncol 2010;28:509–18.
5. Chia S, Gradishar W, Mauriac L, Bines J, Amant F, Federico M, et al. Double-blind, randomized placebo controlled trial of fulvestrant compared with exemestane after prior nonsteroidal aromatase inhibitor therapy in postmenopausal women with hormone receptor-positive, advanced breast cancer: results from EFECT. J Clin Oncol 2008;26:1664–70.
6. Mauri D, Pavlidis N, Polyzos NP, Ioannidis JP. Survival with aromatase inhibitors and inactivators versus standard hormonal therapy in advanced breast cancer: meta-analysis. J Natl Cancer Inst 2006;98:1285–91.
7. Jeselsohn R, Yelensky R, Buchwalter G, Frampton G, Meric-Bernstam F, Gonzalez-Angulo AM, et al. Emergence of constitutively active estrogen receptor-alpha mutations in pretreated advanced estrogen receptor-positive breast cancer. Clin Cancer Res 2014;20:1757–67.
8. Merenbakh-Lamin K, Ben-Baruch N, Yeheskel A, Dvir A, Soussan-Gutman L, Jeselsohn R, et al. D538G mutation in estrogen receptor-alpha: a novel mechanism for acquired endocrine resistance in breast cancer. Cancer Res 2013;73:6856–64.
9. Robinson DR, Wu YM, Vats P, Su F, Lonigro RJ, Cao X, et al. Activating ESR1 mutations in hormone-resistant metastatic breast cancer. Nat Genet 2013;45:1446–51.
10. Toy W, Shen Y, Won H, Green B, Sakr RA, Will M, et al. ESR1 ligand-binding domain mutations in hormone-resistant breast cancer. Nat Genet 2013;45:1439–45.
11. Flanagan JJ, Neklesa TK. Targeting nuclear receptors with PROTAC degraders. Mol Cell Endocrinol 2019;493:110452.
12. McDonnell DP. The molecular pharmacology of estrogen receptor modulators: implications for the treatment of breast cancer. Clin Cancer Res 2005;11:871s–7s.
13. Shah YM, Rowan BG. The Src kinase pathway promotes tamoxifen agonist action in Ishikawa endometrial cells through phosphorylation-dependent stabilization of estrogen receptor (alpha) promoter interaction and elevated steroid receptor coactivator 1 activity. Mol Endocrinol 2005;19:732–48.
14. Viedma-Rodriguez R, Baiza-Gutman L, Salamanca-Gomez F, Diaz-Zaragoza M, Martinez-Hernandez G, Ruiz Esparza-Garrido R, et al. Mechanisms associated with resistance to tamoxifen in estrogen receptor-positive breast cancer (review). Oncol Rep 2014;32:3–15.
15. de Leeuw R, Neefjes J, Michalides R. A role for estrogen receptor phosphorylation in the resistance to tamoxifen. Int J Breast Cancer 2011;2011:232435.
16. Kojetin DJ, Burris TP, Jensen EV, Khan SA. Implications of the binding of tamoxifen to the coactivator recognition site of the estrogen receptor. Endocr Relat Cancer 2008;15:851–70.
17. Fanning SW, Mayne CG, Dharmarajan V, Carlson KE, Martin TA, Novick SJ, et al. Estrogen receptor alpha somatic mutations Y537S and D538G confer breast cancer endocrine resistance by stabilizing the activating function-2 binding conformation. Elife 2016;5:e12792.
18. Toy W, Weir H, Razavi P, Lawson M, Goeppert AU, Mazzola AM, et al. Activating ESR1 mutations differentially affect the efficacy of ER antagonists. Cancer Discov 2017;7:277–87.
19. Katzenellenbogen JA, Mayne CG, Katzenellenbogen BS, Greene GL, Chandarlapaty S. Structural underpinnings of oestrogen receptor mutations in endocrine therapy resistance. Nat Rev Cancer 2018;18:377–88.
20. AstraZeneca. Faslodex (fulvestrant) injection. US prescribing information; 2011. Available from: https://www.accessdata.fda.gov/drugsatfda_docs/label/2011/021344s015lbl.pdf.
21. Perey L, Paridaens R, Hawle H, Zaman K, Nole F, Wildiers H, et al. Clinical benefit of fulvestrant in postmenopausal women with advanced breast cancer and primary or acquired resistance to aromatase inhibitors: final results of phase II Swiss Group for clinical cancer research trial (SAKK 21/00). Ann Oncol 2007;18:64–9.
22. McDonnell DP, Chang CY, Norris JD. Capitalizing on the complexities of estrogen receptor pharmacology in the quest for the perfect SERM. Ann N Y Acad Sci 2001;949:16–35.
23. Wijayaratne AL, Nagel SC, Paige LA, Christensen DJ, Norris JD, Fowlkes DM, et al. Comparative analyses of mechanistic differences among antiestrogens. Endocrinology 1999;140:5828–40.
24. Robertson JFR, Jiang Z, Di Leo A, Ohno S, Pritchard KI, Ellis M, et al. A meta-analysis of clinical benefit rates for fulvestrant 500 mg vs. alternative endocrine therapies for hormone receptor-positive advanced breast cancer. Breast Cancer 2019;26:703–11.
25. van Kruchten M, de Vries EG, Glaudemans AW, van Lanschot MC, van Faassen M, Kema IP, et al. Measuring residual estrogen receptor availability during fulvestrant therapy in patients with metastatic breast cancer. Cancer Discov 2015;5:72–81.
26. Joseph JD, Darimont B, Zhou W, Arrazate A, Young A, Ingalla E, et al. The selective estrogen receptor downregulator GDC-0810 is efficacious in diverse models of ER+ breast cancer. Elife 2016;5:e15828.
27. Lai A, Kahraman M, Govek S, Nagasawa J, Bonnefous C, Julien J, et al. Identification of GDC-0810 (ARN-810), an orally bioavailable selective estrogen receptor degrader (SERD) that demonstrates robust activity in tamoxifen-resistant breast cancer xenografts. J Med Chem 2015;58:4888–904.
28. Weir HM, Bradbury RH, Lawson M, Rabow AA, Buttar D, Callis RJ, et al. AZD9496: an oral estrogen receptor inhibitor that blocks the growth of ER-positive and ESR1-mutant breast tumors in preclinical models. Cancer Res 2016;76:3307–18.
29. Patel HK, Bihani T. Selective estrogen receptor modulators (SERMs) and selective estrogen receptor degraders (SERDs) in cancer treatment. Pharmacol Ther 2018;186:1–24.
30. Traboulsi T, El Ezzy M, Gleason JL, Mader S. Antiestrogens: structure-activity relationships and use in breast cancer treatment. J Mol Endocrinol 2017;58:R15–R31.

31. Kocanova S, Mazaheri M, Caze-Subra S, Bystricky K. Ligands specify estrogen receptor alpha nuclear localization and degradation. BMC Cell Biol 2010;11:98.
32. Kahraman M, Govek SP, Nagasawa JY, Lai A, Bonnefous C, Douglas K, et al. Maximizing ER-alpha degradation maximizes activity in a tamoxifen-resistant breast cancer model: identification of GDC-0927. ACS Med Chem Lett 2019;10: 50–5.
33. Bihani T, Patel HK, Arlt H, Tao N, Jiang H, Brown JL, et al. Elacestrant (RAD1901), a selective estrogen receptor degrader (SERD), has antitumor activity in multiple ER(+) breast cancer patient-derived xenograft models. Clin Cancer Res 2017;23:4793–804.
34. Tria GS, Abrams T, Baird J, Burks HE, Firestone B, Gaither LA, et al. Discovery of LSZ102, a potent, orally bioavailable selective estrogen receptor degrader (SERD) for the treatment of estrogen receptor positive breast cancer. J Med Chem 2018; 61:2837–64.
35. Guan J, Zhou W, Hafner M, Blake RA, Chalouni C, Chen IP, et al. Therapeutic ligands antagonize estrogen receptor function by impairing its mobility. Cell 2019;178:949–63.
36. Ethier SP, Mahacek ML, Gullick WJ, Frank TS, Weber BL. Differential isolation of normal luminal mammary epithelial cells and breast cancer cells from primary and metastatic sites using selective media. Cancer Res 1993;53:627–35.
37. DeRose YS, Wang G, Lin YC, Bernard PS, Buys SS, Ebbert MT, et al. Tumor grafts derived from women with breast cancer authentically reflect tumor pathology, growth, metastasis and disease outcomes. Nat Med 2011;17:1514–20.
38. Bouaboula M, Brollo M, Certal V, El-Ahmad Y, Filoche-Romme B, Halley F, et al. inventors. Novel substituted 6,7-dihydro-5H-benzo[7]annulene compounds, processes for their preparation and therapeutic uses thereof. France patent WO2017140669. 2017.
39. Smith ND, Kahraman M, Govek SP, Nagasawa JY, Lai AG, Bonnefous C, et al. Preparation of substituted 3-[4-[1-(1H-indazol-5-yl)-2-phenylvinyl]phenyl]acrylic acid and derivatives as estrogen receptor modulators. United States patent WO2012037410. 2012.
40. Akhtar N, Bradbury RH, Buttar D, Currie GS, De Savi C, Donald CS, et al. Preparation of (E)-3-[4-(2,3,4,9-tetrahydro-1H-pyrido[3,4-b]indol-1-yl) phenyl]acrylic acid derivatives as antitumor agents. Great Britain patent WO2014191726. 2014.
41. Bouaboula M, Brollo M, Certal V, El-Ahmad Y, Filoche-Romme B, Halley F, et al. Novel substituted N-(3-fluoropropyl)-pyrrolidine compounds, processes for their preparation and therapeutic uses thereof. France patent WO2018091153.20.
42. Dobin A, Davis CA, Schlesinger F, Drenkow J, Zaleski C, Jha S, et al. STAR: ultrafast universal RNA-seq aligner. Bioinformatics 2013;29:15–21.
43. Trapnell C, Williams BA, Pertea G, Mortazavi A, Kwan G, van Baren MJ, et al. Transcript assembly and quantification by RNA-seq reveals unannotated transcripts and isoform switching during cell differentiation. Nat Biotechnol 2010;28: 511–5.
44. Lin CY, Strom A, Vega VB, Kong SL, Yeo AL, Thomsen JS, et al. Discovery of estrogen receptor alpha target genes and response elements in breast tumor cells. Genome Biol 2004;5:R66.
45. Welboren WJ, Stunnenberg HG, Sweep FC, Span PN. Identifying estrogen receptor target genes. Mol Oncol 2007;1:138–43.
46. Wardell SE, Nelson ER, Chao CA, Alley HM, McDonnell DP. Evaluation of the pharmacological activities of RAD1901, a selective estrogen receptor degrader. Endocr Relat Cancer 2015;22:713–24.
47. Brunner N, Frandsen TL, Holst-Hansen C, Bei M, Thompson EW, Wakeling AE, et al. MCF7/LCC2: a 4-hydroxytamoxifen resistant human breast cancer variant that retains sensitivity to the steroidal antiestrogen ICI 182,780. Cancer Res 1993; 53:3229–32.
48. Casa AJ, Potter AS, Malik S, Lazard Z, Kuiatse I, Kim HT, et al. Estrogen and insulin-like growth factor-I (IGF-I) independently down-regulate critical repressors of breast cancer growth. Breast Cancer Res Treat 2012;132:61–73.
49. Liao GJ, Clark AS, Schubert EK, Mankoff DA. 18F-fluoroestradiol PET: current status and potential future clinical applications. J Nucl Med 2016;57:1269–75.
50. Sikora MJ, Cooper KL, Bahreini A, Luthra S, Wang G, Chandran UR, et al. Invasive lobular carcinoma cell lines are characterized by unique estrogen-mediated gene expression patterns and altered tamoxifen response. Cancer Res 2014;74:1463–74.
51. Ponnusamy S, Asemota S, Schwartzberg LS, Guestini F, McNamara KM, Pierobon M, et al. Androgen receptor is a non-canonical inhibitor of wild-type and mutant estrogen receptors in hormone receptor-positive breast cancers. iScience. 2019;21:341–58.
52. Hanzelmann S, Castelo R, Guinney J. GSVA: gene set variation analysis for microarray and RNA-seq data. BMC Bioinformatics 2013;14:7.
53. El-Ahmad Y, Tabart M, Halley F, Certal V, Thompson F, Filoche-Romme B, et al. Discovery of 6-(2,4-dichlorophenyl)-5-[4-[(3S)-1-(3-fluoropropyl)pyrrolidin-3-yl]oxyphenyl]-8, 9-dihydro-7H-benzo[7]annulene-2-carboxylic acid (SAR439859), a potent and selective estrogen receptor degrader (SERD) for the treatment of estrogen-receptor-positive breast cancer. J Med Chem 2020;63: 512–28.
54. Wardell SE, Yllanes AP, Chao CA, Bae Y, Andreano KJ, Desautels TK, et al. Pharmacokinetic and pharmacodynamic analysis of fulvestrant in preclinical models of breast cancer to assess the importance of its estrogen receptor-alpha degrader activity in antitumor efficacy. Breast Cancer Res Treat 2020; 179:67–77.